Available online at www.sciencedirect.com

ScienceDirect

Journal of the European Ceramic Society 34 (2014) 1741–1753

www.elsevier.com/locate/jeurceramsoc

Origin of extrinsic dielectric loss in 1:2 ordered, single-phase $BaMg_{1/3}Ta_{2/3}O_3$

T. Kolodiazhnyi *

National Institute for Materials Science, 1-1 Namiki, Tsukuba, Ibaraki 305-0044, Japan

Received 1 October 2013; received in revised form 20 December 2013; accepted 23 December 2013
Available online 18 January 2014

Abstract

Among the family of temperature-compensated microwave dielectric ceramics, $BaMg_{1/3}Ta_{2/3}O_3$ shows the lowest dielectric loss and remains a material of choice for state-of-the-art airborne and land-based communication systems. We report on the compositional stability range, microwave dielectric properties, and the degree of atomic order of the title compound within the BaO–MgO–Ta_2O_5 ternary diagram. In most cases an atomic order is robust to the deviation from stoichiometry with an exception of Ba-rich and/or Ta-deficient samples which favor (partial) disorder. We further demonstrate that the dense, atomically ordered $BaMg_{1/3}Ta_{2/3}O_3$ ceramic shows large variation of dielectric loss within a single phase composition region – a clear message that the dielectric loss in practical ceramics is dominated by extrinsic sources and that the cation order alone is insufficient to achieve a minimum dielectric loss in $BaMg_{1/3}Ta_{2/3}O_3$. The low-temperature dielectric relaxation studies suggest that the extrinsic dielectric loss in the title compound is due to the 'rattling' of the off-centered Mg^{2+} ions misplaced at the Ba sites. Controlled deviation from the $BaMg_{1/3}Ta_{2/3}O_3$ stoichiometry toward the Mg-deficient region leads to suppression of the extrinsic dielectric loss as a result of the reduced chemical activity of Mg ion.

Keywords: Microwave ceramics; Point defects; Dielectric loss; Phase equilibria

1. Introduction

$BaMg_{1/3}Ta_{2/3}O_3$, herein abbreviated as BMT, belongs to a group of complex perovskites with a general formula $Ba(B'_{1/3}B''_{2/3})O_3$, where B′ and B″ are di- and penta-valent cations, respectively.[1] Stoichiometric BMT crystallizes in a trigonally distorted 1:2 ordered perovskite structure ($P\bar{3}m1$ space group) similar to that of the prototypical $BaSr_{1/3}Ta_{2/3}O_3$ compound.[2] These results are also supported by numerous theoretical studies which suggest that the ground state of the $Ba(B'_{1/3}B''_{2/3})O_3$ perovskites has 1:2 B-site cation ordered configuration along the ⟨111⟩ direction of pseudo-cubic perovskite unit cell.[3–8]

BMT ceramics[9] along with $BaZn_{1/3}Ta_{2/3}O_3$ and $BaZn_{1/3-x}Co_xNb_{2/3}O_3$ satisfy three important requirements for applications in microwave dielectric resonator (DR): (*i*) low dielectric loss, tan δ, or high Q-factor ($Q \geq 7000$ where $Q \approx 1/\tan\delta$), (*ii*) relatively high dielectric constant, ε' ($20 < \varepsilon' < 40$) and (*iii*) small and tunable temperature coefficient of the resonance frequency, τ_f ($0 < \tau_f < 6$ ppm/K).

By definition, the Q-factor is a ratio of the energy stored in the resonant cavity over the energy dissipated per one cycle of electromagnetic wave oscillation. Owing to its highest Q-factor among the known DR materials, BMT offers the most efficient utilization of the allocated frequency band. Nowadays BMT DRs are used in GPS and communication satellites, phase-locked DR oscillators and microwave band-pass filters with low insertion loss.[10]

From an academic viewpoint, BMT is an important compound that continues to challenge our ability to understand and predict the dielectric loss in microwave ceramics.[11] After 3 decades of research, however, it is still unclear what are the main sources of extrinsic dielectric loss in BMT and what has to be done to eliminate these sources during preparation of ceramics.

Based on the theories of microwave dielectric loss it is generally believed that dense, single-phase, stoichiometric $Ba(B'_{1/3}B''_{2/3})O_3$ with minimum internal lattice strain, high degree of 1:2 B-site cation order and low concentration of 0-, 1-, and 2-dimensional defects will possess the lowest tan δ which is limited only by the intrinsic damping of the optical phonons.[12,13]

* Tel.: +81 29 860 4407; fax: +81 29 860 4706.
E-mail address: kolodiazhnyi.taras@nims.go.jp

0955-2219/$ – see front matter © 2014 Elsevier Ltd. All rights reserved.
http://dx.doi.org/10.1016/j.jeurceramsoc.2013.12.037

Large volume of literature related to preparation of the low-loss BMT has emphasized the importance of 'sintering aids' and dopants claiming that they are necessary to achieve the BMT with low dielectric loss. A few examples of these dopants include Ti, Zn, Ca, Sr, W, Nb, Zr, Mn, Sn, P, Sb, Ga, K, Na, Co, Ni and rare earths.[14–22]

First-principles calculations of the $Ba(B'_{1/3}B''_{2/3})O_3$ phase stability range[8] predict the atomic disorder in BMT to occur above 3080 °C. Therefore, it was recommended to sinter BMT for a long period of time at the highest possible temperature to enhance the degree of the 1(Mg):2(Ta) cation order.[8] In contrast to these theoretical forecasts it was found that during high temperature treatment ($T \geq 1650$ °C) stoichiometric BMT starts to decompose and shows traces of Ta-rich second phase.[16,23–25]

A common wisdom suggests that the lowest tanδ should be attained in stoichiometric ceramics, i.e., in compounds with the lowest concentration of intrinsic lattice defects.[12] Fujimaru et al.[26] studied the response of the dielectric properties of BMT to a small deviation from stoichiometry. In contrast to expectations, the highest-Q BMT was found far from stoichiometric composition. In particular, the target compositions of high-Q ceramics were rich in Ba and Ta and significantly depleted in Mg.[26] Somewhat similar results were obtained by Surendran et al.[27] for $Ba_{1-x}(Mg_{1/3-y}Ta_{2/3})O_3$. Related works on the $BaZn_{1/3}Ta_{2/3}O_3$ (BZT),[28,29] $BaZn_{1/3}Nb_{2/3}O_3$ (BZN),[30] $BaMg_{1/3}Nb_{2/3}O_3$ (BMN),[31,32] and $BaCo_{1/3}Nb_{2/3}O_3$ (BCN),[32,33] have also found Q-factor enhancement in the B′-deficient non-stoichiometric compositions.

Depending on a specific perovskite, e.g., BZT, BZN, BMT or BMN, slight deviation from stoichiometry may have a profound effect on the degree of the 1:2 cation ordering.[27–30] Large Q-factor variation within dense, highly ordered BZT was reported by Koga et al.[29] Wu and Davies demonstrated that the high degree of the 1:2 order in the non-stoichiometric BZN leads to the highest Q-factor.[30] On the other hand, very high Q-factors have been achieved in non-stoichiometric disordered BMT- and BMN-based perovskites.[14,34]

This paper addresses several issues. First, the effect of BMT non-stoichiometry on the Q-factor is explored in detail. Second, a compositional range corresponding to a single-phase BMT and the solubility limit of native point defects are addressed. Next, possible correlations between the Q-factor, composition, 1:2 cation order, trigonal lattice distortions and atomic bond lengths are discussed. Finally, the author outlines a point defect model that explains the origin of extrinsic dielectric loss and a large Q-factor variation in the non-stoichiometric, single-phase, 1:2 ordered BMT.

2. Experimental

Samples were prepared from well-dried 99.9% pure $BaCO_3$ (Wako Chemicals), 99.99 % MgO and 99.9% Ta_2O_5 (Tokai Chemy). The allocated amounts of powder were weighed on analytical balance with an error not exceeding ±3 mg. Each batch contained around 20 g of powder. An error between the actual and the target sample compositions was estimated to be below ±0.2 mol%.

The powders were mixed in ethanol with zirconia balls on rollers at 80 rpm for 20 h. Powders were calcined in air at 1200 °C for 5 h. Green cylindrical pellets of 7 mm diameter were pressed under 1000 kg/cm^2 uniaxial pressure using WC pressing dies (Fuji Die Co. Ltd., Japan). Sintering of BMT samples was performed at 1580–1680 °C for 5–100 h in static air in electrical furnace (Koyo, Japan).

Phase purity and lattice parameters of the sintered samples were analyzed by X-ray powder diffraction (Rigaku Ultima III with Cu K_α X-ray source). Structural parameters were obtained from Rietveld refinement of the X-ray data using RIETAN 2000.[35] Lattice parameters and Wyckoff site and atomic fractional coordinates were initiated by using the BMT structural data from Ref. 36. The X-ray powder diffraction profiles were refined in the range of $10° < 2\Theta < 140°$. During refinement, atomic thermal factors, B, for weak X-ray scattering elements such as, O1(3e), O2(6i) and Mg(1b) were fixed, while the B factors for Ba1(1a), Ba2(2d) and Ta(2d) were relaxed and successfully refined to positive values. To estimate the degree of B-site cation disorder, the occupancies of the B-site cations were relaxed under constraint $g[Mg(1b)]\times 1 + g[Mg(2d)]\times 2 = 1$ and $g[Ta(1b)]\times 1 + g[Ta(2d)]\times 2 = 2$, where g is the fractional occupancy of the ion whose Wyckoff site is shown in brackets. For complete 1:2 cation order, $g[Mg(1b)] = 1$ and $g[Ta(2d)] = 1$. For complete disorder, $g[Mg(1b)] = 0.333$ and $g[Ta(2d)] = 0.666$. The B factors of the atoms occupying the same Wyckoff sites were set to be equal, namely, $B[Mg(1b)] = B[Ta(1b)]$ and $B[Ta(2d)] = B[Mg(2d)]$.

Microstructure of both polished and thermally etched sintered ceramics were determined with Hitachi S-4800 scanning electron microscope equipped with energy dispersive X-ray spectrometer (HORIBA Emax).

The MW measurements were performed in the frequency range of 10–10.5 GHz. For microwave dielectric measurements the diameter-to-thickness ratio of the DR was adjusted to ≈2.26 to make certain that the first resonance mode is of the $TE_{01\delta}$-type. The DR was placed on the low-loss quartz support of 5 mm diameter and 4.3 mm height in the center of the silver-clad cylindrical resonance cavity (QWED, Poland) having inner diameter of 24 mm and height of 16 mm. The microwave resonances in transmission mode (s^{21} parameter) were measured using HP 8719C vector network analyzer. The dielectric constant, ε' was calculated using the QWED software[37] which takes into account the geometry of the DR and the metal enclosure. The unloaded Q-factor was calculated according to:

$$Q = \frac{Q_L}{1 - 10^{-P/20}} \quad (1)$$

where Q_L is the loaded quality factor determined from the full width of the resonance peak at the 3 dB level, and P is the absolute value of the s^{21} parameter at the resonance in dB. To minimize the coupling, the s^{21} parameter at the resonance peak was adjusted to around −30 dB. Because no corrections for conduction loss were included in the calculations, the $Q \times f$ reported in Table 1 represent the lower bound value. Temperature coefficient of the resonance frequency, τ_f, was measured in the

Table 1
Selected target compositions, lattice parameters and dielectric properties of the studied compounds. Capital letters in the sample's abbreviation indicates the compatibility triangle as discussed in the text. Compounds containing secondary phases are marked by asterisk. Chemical composition values x, y and z are given in mole. Dielectric data for samples located in the D, E, and F CTs could not be measured due to the very low density of ceramics. Numbers in brackets represent one standard deviation. Because of significant degree of disorder and poor fit by Rietveld refinement, the Mg(1b) site occupancy by Mg ion, g[Mg(1b)], for samples D16–D18 and E15 were calculated using Eq. (4) as discussed in the text.

Sample	BaO x	MgO y	Ta_2O_5 z	a (Å)	c (Å)	c/a	Vol (Å^3)	g[Mg(1b)] (%)	ε'	$Q \times f$ (THz)	τ_f (ppm/°C)
BMT	0.6	0.2	0.2	5.77233(8)	7.0931(11)	1.2288	204.679(6)	98.9(3)	24.3	40.1	2.0
A10*	0.5999	0.1939	0.2062	5.7721(14)	7.0931(18)	1.2288	204.664(9)	98.7(3)	25.8	41.6	24.3
A11*	0.6034	0.1932	0.2034	5.7735(11)	7.0967(14)	1.2292	204.867(7)	99.3(4)	24.7	160	5.29
B7*	0.5928	0.2036	0.2036	5.7713(10)	7.0920(14)	1.2288	204.575(7)	101.7(5)	24.5	11.0	7.96
B9*	0.5975	0.1956	0.2069	5.7724(14)	7.0933(18)	1.2288	204.691(9)	100.0(3)	25.7	30.6	18.8
C1	0.5975	0.2031	0.1994	5.77109(9)	7.0898(12)	1.2285	204.494(6)	98.2(3)	24.3	30.0	2.3
C2*	0.5892	0.2110	0.1998	5.77070(7)	7.09071(9)	1.2287	204.493(5)	101.2(3)	24.3	20.1	2.3
C3*	0.5836	0.2169	0.1995	5.77084(7)	7.09057(9)	1.2287	204.498(6)	101.3(3)	23.8	14.0	1.7
C6	0.5942	0.2062	0.1996	5.77201(5)	7.09222(6)	1.2287	204.629(3)	100.4(3)	24.3	20.7	2.3
D16*	0.6058	0.2002	0.1940	5.7785(2)	7.0865(3)	1.2264	204.92(13)	81.3(9)	–	–	–
D17*	0.6022	0.2045	0.1933	5.7788(15)	7.0885(3)	1.2268	204.89(12)	83.8(9)	–	–	–
D18*	0.5975	0.2069	0.1956	5.767(14)	7.073(18)	1.2264	203.8(10)	84.8(9)	–	–	–
E14*	0.6070	0.1950	0.1980	5.7638(8)	7.080(10)	1.2285	203.72(6)	97.9(8)	–	–	–
E15*	0.6070	0.1965	0.1965	5.7773(9)	7.0886(15)	1.2269	204.900(14)	83.6(10)	–	–	–
E30	0.6010	0.1995	0.1995	5.7723(10)	7.0900(13)	1.2283	204.584(7)	97.6(4)	–	–	–
F13	0.6064	0.1937	0.1999	5.77225(8)	7.0921(10)	1.2287	204.643(5)	99.2(3)	–	–	–
F25*	0.6022	0.1979	0.1999	5.77369(9)	7.0937(12)	1.2286	204.735(6)	98.3(3)	–	–	–
F28*	0.6028	0.1976	0.1996	5.77301(9)	7.0934(12)	1.2287	204.791(7)	99.1(3)	–	–	–
G19	0.6046	0.1951	0.2003	5.7752(11)	7.0958(14)	1.2287	204.962(7)	98.7(4)	24.4	235	2.6
G34	0.6080	0.1903	0.2017	5.77485(9)	7.0976(13)	1.2291	204.985(6)	99.0(3)	24.5	280	3.53
G39	0.6066	0.192	0.2014	5.7748(10)	7.0972(13)	1.2290	204.967(7)	99.1(3)	24.4	270	3.18
G63	0.6039	0.1960	0.2001	5.77315(7)	7.09222(9)	1.2285	204.710(5)	99.2(4)	24.3	228	2.72
G87*	0.6141	0.1858	0.2001	5.7757(13)	7.0961(17)	1.2286	205.001(9)	98.5(3)	24.8	192	3.91
G89	0.6110	0.1887	0.2003	5.7744(10)	7.0963(14)	1.2289	204.917(7)	99.0(4)	24.8	264	3.17
H36	0.6064	0.1903	0.2033	5.77533(9)	7.0985(12)	1.2291	205.047(6)	99.2(3)	24.5	281	3.68
H41	0.6050	0.1930	0.2020	5.77275(5)	7.09552(8)	1.2291	204.776(3)	100.8(3)	24.6	325	3.13
H48*	0.6080	0.1875	0.2045	5.7743(13)	7.0974(18)	1.2291	204.936(9)	100.0(4)	24.6	285	4.85
H51	0.6050	0.1920	0.2030	5.77401(9)	7.0973(12)	1.2292	204.916(6)	100.6(3)	24.6	330	3.24
H60	0.6030	0.1950	0.2020	5.7727(10)	7.0950(13)	1.2291	204.757(8)	100.9(3)	24.5	340	2.9
H61	0.6040	0.1940	0.2020	5.77443(9)	7.0973(12)	1.2291	204.948(6)	100.3(3)	24.5	330	3.07
H70	0.6018	0.1976	0.2006	5.77277(8)	7.0936(11)	1.2288	204.723(6)	98.9(3)	24.3	260	2.8
H86*	0.6067	0.1895	0.2038	5.7735(13)	7.0970(17)	1.2292	204.872(9)	100.2(3)	24.6	290	4.1
H88*	0.6135	0.1779	0.2086	5.7733(18)	7.0960(3)	1.2291	204.83(13)	101.3(4)	25.3	200	7.13

temperature interval of +20 to +90 °C and obtained according to:

$$\tau_f = \frac{\Delta f}{f_0 \times \Delta T}, \quad (2)$$

where Δf is a shift of the resonant frequency, f_0, introduced by a temperature change of ΔT.

Dielectric properties in the 500 Hz to 1 MHz frequency range were measured with Agilent E4980 Precision LCR Meter in a home-made sample cell mounted on the probe head of the physical property measurements system (PPMS, Quantum Design).[38]

3. Results and discussion

3.1. Thermodynamic phase equilibria and density

Revised subsolidus phase equilibria in the BaO–MgO–Ta_2O_5 system has been reported by Kolodiazhnyi et al.[39] Below 1650 °C there are three thermodynamically stable ternary compounds: $BaMg_{1/3}Ta_{2/3}O_3$, $Ba_9MgTa_{14}O_{45}$, and $Ba_4MgTa_{10}O_{30}$. The $Ba_9MgTa_{14}O_{45}$ phase with tetragonal-tungsten bronze (TTB) structure first reported by Kryshtop et al.[40] is a relaxor-type dielectric[41,42] characterized by high dielectric loss that causes significant degradation of the Q-factor in BMT-based DRs. Traces of $Ba_9MgTa_{14}O_{45}$ second phase erroneously identified as either $BaTa_2O_6$ or $Ba_3Ta_5O_{15}$ were reported in a study of BMT ceramic sintered at 1600–1700 °C.[16,23–25] Confusion in identification of this phase in early reports can be explained by the fact that $Ba_9MgTa_{14}O_{45}$ is isostructural with both the TTB-type $Ba_3Ta_5O_{15}$ and $BaTa_2O_6$ and contains only a small amount of Mg – a light scattering element which is difficult to detect with energy dispersive X-ray spectroscopy and X-ray diffraction techniques. Comprehensive analysis of structural, dielectric and Raman properties of the $Ba_4MgTa_{10}O_{30}$ incipient ferroelectric compound that forms in the Ta_2O_5-rich part of the BaO–MgO–Ta_2O_5 ternary diagram has been reported recently in Ref. 43. In addition to the three ternary phases discussed above, a metastable high-temperature 10-layer hexagonal perovskite phase $Ba_{10}Mg_{2.5x}Ta_{8-x}O_3$ with x = 0-1.333 has been reported by Mallinson et al.[44]

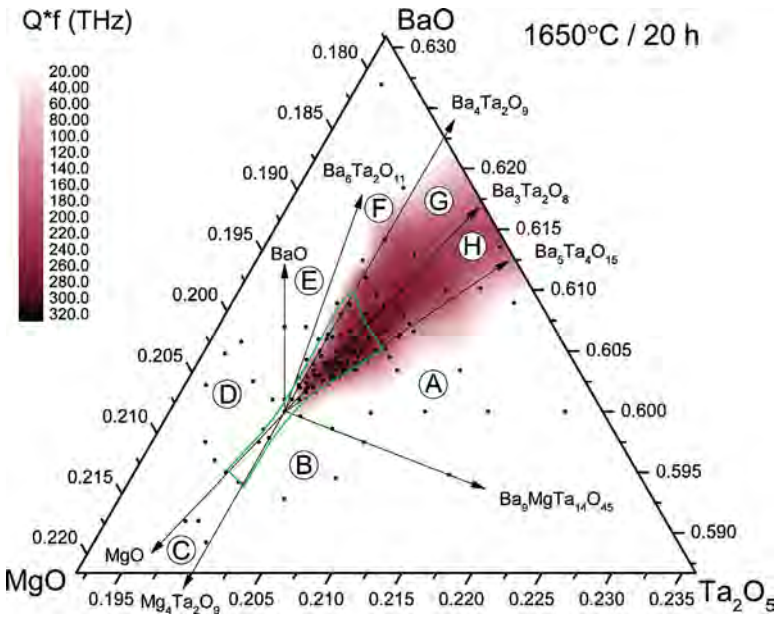

Fig. 1. Part of the BaO–MgO–Ta_2O_5 phase diagram in the vicinity of the BMT phase indicating a composition dependence of the $Q \times f$ for samples sintered at 1650 °C for 20 h. Small black dots indicate the target sample compositions. Green line indicates an approximate boundary of the single-phase BMT. (For interpretation of the references to color in this figure legend, the reader is referred to the web version of the article.)

In equilibrium, BMT forms tie lines with five thermodynamically stable compounds, such as $Ba_5Ta_4O_{15}$, MgO, BaO, $Ba_9MgTa_{14}O_{45}$ and $Mg_4Ta_2O_9$. In addition, three metastable compounds, $Ba_6Ta_2O_{11}$, $Ba_4Ta_2O_9$ and $Ba_3Ta_2O_8$ reported by Kovba et al.,[45–47] have been also considered in this work. For convenience, the studied chemical compositions are assigned to compatibility triangles in the BaO–MgO–Ta_2O_5 ternary phase diagram adopted from Ref. [39] (see Fig. 1). These compatibility triangles further abbreviated as CTs include:

A: $BaMg_{1/3}Ta_{2/3}O_3$–$Ba_5Ta_4O_{15}$–$Ba_9MgTa_{14}O_{45}$
B: $BaMg_{1/3}Ta_{2/3}O_3$–$Ba_9MgTa_{14}O_{45}$–$Mg_4Ta_2O_9$
C: $BaMg_{1/3}Ta_{2/3}O_3$–$Mg_4Ta_2O_9$–MgO
D: $BaMg_{1/3}Ta_{2/3}O_3$–MgO–BaO
E: $BaMg_{1/3}Ta_{2/3}O_3$–BaO–$Ba_6Ta_2O_{11}$
F: $BaMg_{1/3}Ta_{2/3}O_3$–$Ba_6Ta_2O_{11}$–$Ba_4Ta_2O_9$
G: $BaMg_{1/3}Ta_{2/3}O_3$–$Ba_4Ta_2O_9$–$Ba_3Ta_2O_8$
H: $BaMg_{1/3}Ta_{2/3}O_3$–$Ba_3Ta_2O_8$–$Ba_5Ta_4O_{15}$.

Ceramic samples whose chemical composition falls within the A, B and C CTs reach the relative density of 96–98% after sintering at 1550–1580 °C for 20 h. Samples located in the H and G CTs required sintering at 1630–1650 °C to reach the relative density of 96–98%. The specimens located in the D, E and F CTs remained ≤80% dense after heat treatment at 1680 °C.

3.2. Chemical composition and dielectric properties

Several representative examples of the studied compositions are summarized in Table 1. According to Fig. 1 and Table 1, stoichiometric BMT sintered at 1650 °C for 20 h shows a poor dielectric performance with $Q \times f \approx 20$–40 THz. A very strong variation of the dielectric properties and density of ceramics was found upon slight deviation from the stoichiometric BMT composition.

Ta-poor non-stoichiometric BMT samples located in the D, E and F CTs showed very low density after sintering at 1650 °C for 20 h. Because of the low electric filling factor of the DR, no electromagnetic resonance peaks were detected in the microwave range of 8–13 GHz. As a result, no microwave dielectric data are reported for these samples in Table 1. Attempts to improve the density of these ceramics were unsuccessful; the samples have reached the maximum density of ≤80% after sintering at 1680 °C for 50 h. This density, however, was insufficient to detect an electromagnetic resonance.

Significant improvement in the Q-factor is seen for samples with a slight Mg deficiency which are located in the G and H CTs (Fig. 1). The data for samples H51, H60, H61 in Table 1 reveal that the highest $Q \times f$ of 330–340 THz were found for Mg-deficient BMT samples with chemical composition within the H CT close to the $BaMg_{1/3}Ta_{2/3}O_3$–$Ba_3Ta_2O_8$ tie line. Upon approaching the BMT–$Ba_5Ta_4O_{15}$ tie line from the H CT, the $Q \times f$ starts to decrease and drops sharply after crossing into the A CT. The decrease in the $Q \times f$ values for samples located in the A CT can be explained by the appearance of the $Ba_9MgTa_{14}O_{45}$ second phase with TTB structure. In the specimens located very close to the BMT–$Ba_5Ta_4O_{15}$ tie line the trace amount of the TTB phase could not be detected by powder X-ray diffraction. Yet, undetectable traces of $Ba_9MgTa_{14}O_{45}$ are responsible for an increase in the temperature coefficient of the resonant frequency, τ_f. A single-phase BMT has $\tau_f = +2, \ldots, +2.5$ ppm/°C. As the Ta_2O_5 content increases in the samples located in the A CT, so does the τ_f. For example, sample A10 in Table 1 shows $\tau_f = +24.3$ ppm/°C and $Q \times f = 42$ THz. Clear evidence of the $Ba_9MgTa_{14}O_{45}$ second phase in the powder X-ray diffraction pattern of sample A10 is shown in Fig. 2.

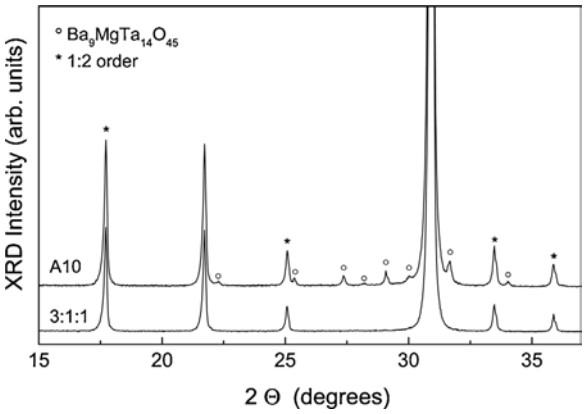

Fig. 2. X-ray diffraction patterns of the A10 and stoichometric BMT abbreviated as 3:1:1. Both samples sintered at 1650 °C for 20 h. Open circles indicate X-ray reflections from $Ba_9MgTa_{14}O_{45}$ second phase. Asterisks indicate reflections associated with the 1:2 cation order of BMT phase.

Surprisingly low $Q \times f$ values (e.g., $Q \times f \leq 20$ THz) were found in the Mg-rich BMT with the target compositions located within the B and C CTs. This result is difficult to understand because the samples from the B and C CTs demonstrated high density and high degree of 1:2 cation order as discussed latter in the text. While the low Q in the B CT can be partially attributed to the possible presence of the $Ba_9MgTa_{14}O_{45}$ second phase below the X-ray detection limit, the latter phase does not exist in the samples equilibrated in the C CT. The only two second phases that form in the C CT are $Mg_4Ta_2O_9$ and MgO. Both phases show very low dielectric loss. In particular, literature data indicates that $Mg_4Ta_2O_9$ has $Q \times f = 350$ THz[48] and MgO has $Q \times f \approx 400$ THz.[49] In fact, the low-loss Nb-based analog of corundum-type $Mg_4Ta_2O_9$ phase has been used by the author for tuning the τ_f in the $BaMg_{1/3}Nb_{2/3}O_3$–$Mg_4Nb_2O_9$ composite dielectric resonators sintered at 1320 °C.[50] A possible origin of extrinsic dielectric loss in the Mg-rich BMT samples is discussed later in the text based on the point defect model involving partial accommodation of Mg at Ba-site.

Overall, with several important exceptions, our results on compositional dependence of the Q-factor are in qualitative agreement with those reported by Fujimaru et al.[26] Both results indicate that the high-Q BMT ceramics are located in the Mg-deficient composition field. However, in contrast to Fujimaru et al.[26], whose highest-Q samples (e.g., $Q \times f = 298$ THz) are reported within the A CT close to the BMT–$Ba_5Ta_4O_{15}$ tie line, none of our samples located in the A compatibility triangle show $Q \times f$ greater than 200 THz. Instead, the best performing samples found in this study, e.g., those with $Q \times f > 320$ THz, are located in the H CT. Again, in contrast to Fujimaru et al, our data indicate a pronounced decrease in the Q-factor upon approaching the BMT–$Ba_5Ta_4O_{15}$ tie line from the H CT and crossing into the A CT (Fig. 1). In author's opinion, a sudden drop in the Q-factor in the A CT is due to the presence of the TTB-type $Ba_9MgTa_{14}O_{45}$ second phase.[40] The results in Fig. 1 are also in good agreement with the data reported by Ohsato et al.[51] for non-stoichiometric BMT sintered at 1600 °C for 20 h. The main differences with the latter report may be attributed to the higher sintering temperatures employed in the present work.

3.3. Solubility limit of native point defects

Depending on preparation conditions and chemical substitution with hetero-valent ions, perovskites can accommodate significant concentrations of native point defects, such as cation and anion vacancies as well as misplaced ions.[52–55] Because defect formation is a thermally activated process, equilibrium concentration of point defects increases exponentially with temperature. Although significant progress has been made in understanding of the point defect chemistry in simple perovskites such as $SrTiO_3$[56] and $BaTiO_3$,[57] thermodynamics of point defects in more complex perovskites, including solid solutions of simple perovskites, remains an extremely challenging task.[58,59] While a complete picture of the point defect chemistry of BMT is beyond the scope of this paper, the author will focus on several types of point defects that may critically affect the dielectric loss in the BMT ceramics. Because there are no data on the defect energies in BMT, the author will refer, whenever appropriate, to the literature data available for simple perovskites.

There are numerous methods to determine the homogeneity limits of the single phase compound; these include, for example, microscopical or powder diffraction detection of the second phases. Also, very accurate methods are based on the resonant or non-resonant magnetic measurements in those cases when the second phase happens to be magnetically active.[60–62] In most critical cases of this study, the evolution of the unit cell lattice parameters was analyzed upon deviation from stoichiometric BMT. Within this method the solubility limit of the native point defects is reached when the unit cell becomes invariant to further deviation from stoichiometry.[63] In addition to its high accuracy, this method is particularly suitable when the minute amount of the second phases such as, $Mg(OH)_2$, MgO, and amorphous-like BaO are difficult to detect by electron microscopy or diffraction techniques. An approximate boundary of the BMT single-phase region determined this way is outlined by the green line in Fig. 1.

The solubility of point defects in BMT is quite small but it extends noticeably along the BMT–$Ba_4Ta_2O_9$, BMT–$Ba_3Ta_2O_8$, and BMT–$Ba_5Ta_4O_{15}$ tie lines. Somewhat smaller solubility is found along the BMT–$Mg_4Ta_2O_9$ and BMT–MgO pseudo-binaries. Negligible homogeneity range of BMT solid solution was found along the BaO and $Ba_6Ta_2O_{11}$ joints (see Fig. 1).

As a way of example, we focus on defect solubility limit, lattice parameters, atomic order and dielectric properties of non-stoichiometric BMT samples formulated along the $Mg_4Ta_2O_9$–$Ba_4Ta_2O_9$ tie line. For convenience, the chemical composition along this joint is represented by a hypothetical formula: $Ba_{4-5y}Mg_{5y}Ta_2O_9$. For $y = 0.2$ the compound is stoichiometric BMT. For $y < 0.2$ the BMT compositions are Mg-poor, whereas for $y > 0.2$ they are Mg-rich.

Selected X-ray diffraction patterns of the $Ba_{4-5y}Mg_{5y}Ta_2O_9$ compositions are shown in Fig. 3. Mg-excess samples with $y > 0.2062$ show additional X-ray peaks associated with $Mg_4Ta_2O_9$ second phase. Mg-poor samples with $y < 0.1887$

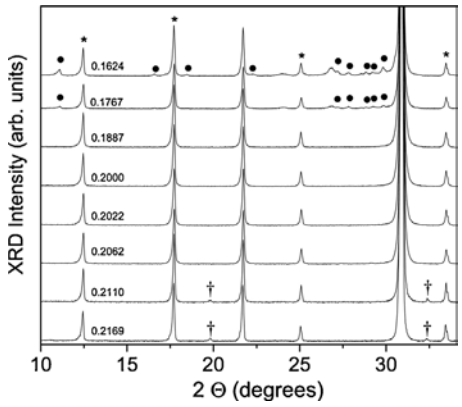

Fig. 3. Part of the X-ray diffraction patterns of the $Ba_{4-5y}Mg_{5y}Ta_2O_9$ samples along the $Mg_4Ta_2O_9$–$Ba_4Ta_2O_9$ tie line. Numbers above each pattern indicate the value of y. Daggers indicate reflections from the $Mg_4Ta_2O_9$ second phase. Dots indicate X-ray reflections from the $Ba_4Ta_2O_9$ second phase. Asterisks indicate reflections associated with the 1:2 cation order of the main BMT phase.

show traces of metastable $Ba_4Ta_2O_9$ phase and additional traces of $BaCO_3$ and $Ba_3Ta_2O_8$ which are the products of decomposition of the $Ba_4Ta_2O_9$ phase.

Fig. 4 shows an evolution of the lattice parameters (unit cell a and c, and unit cell volume, V) of the samples along the $Mg_4Ta_2O_9$–$Ba_4Ta_2O_9$ pseudo-binary. For all the chemical compositions included in Fig. 4 the maximum deviation from the $Mg_4Ta_2O_9$–$Ba_4Ta_2O_9$ tie line does not exceed the sample preparation uncertainty of ±0.2 mol%. Saturation of the a, c, and V at $y \geq 0.2065$ and $y \leq 0.1911$ (marked by vertical solid lines in Fig. 4) indicates the solubility limit of the native point defects in BMT along the $Mg_4Ta_2O_9$–$Ba_4Ta_2O_9$ tie line. Upon departure from stoichiometry, Mg-deficient BMT ceramics show an increase in the unit cell volume, whereas Mg-rich BMT shows a decrease in V. It is important to note a strong $Q \times f$ compositional variation from 30 to 260 THz within a *single-phase* BMT region along the $Mg_4Ta_2O_9$–$Ba_4Ta_2O_9$ joint (Fig. 4d). Also note that the degree of the 1:2 cation order, as reflected in the Mg-site occupancy by Mg ion, g[Mg(1b)], obtained from Rietveld refinement of the single-phase BMT is essentially the same, i.e., g[Mg(1b)] = 99.0 ± 1% (Fig. 4e). This is a clear message that the high degree of the 1:2 atomic order is *insufficient* to achieve a high-Q BMT. Similar point has already been noticed by Koga et al. in the study of the non-stoichiometric BZT.[28,29]

Fig. 5 shows scanning electron microscopy (SEM) images of polished (panels a, c, e, and g), and thermally etched (panels b, d, f, and h) surfaces of $Ba_{4-5y}Mg_{5y}Ta_2O_9$ ceramics along the $Mg_4Ta_2O_9$–$Ba_4Ta_2O_9$ tie line, where $y = 0.211$ (panels a and b), $y = 0.2022$ (panels c and d), $y = 0.2$ (panels e and f), $y = 0.192$ (panels g and h). Please note that Mg-rich BMT ceramics with $y = 0.211$ shows a multi-phase composition with a second phase, $Mg_4Ta_2O_9$, marked by white arrows in panel a of Fig. 5. There is also a noticeable compositional dependence of the grain size (see Fig. 5 panels b, d, f, and h). The average grain size decreases with the decrease in Mg concentration along the $Mg_4Ta_2O_9$–$Ba_4Ta_2O_9$ tie line. For detailed crystal and dielectric data of these ceramics please refer to Fig. 4.

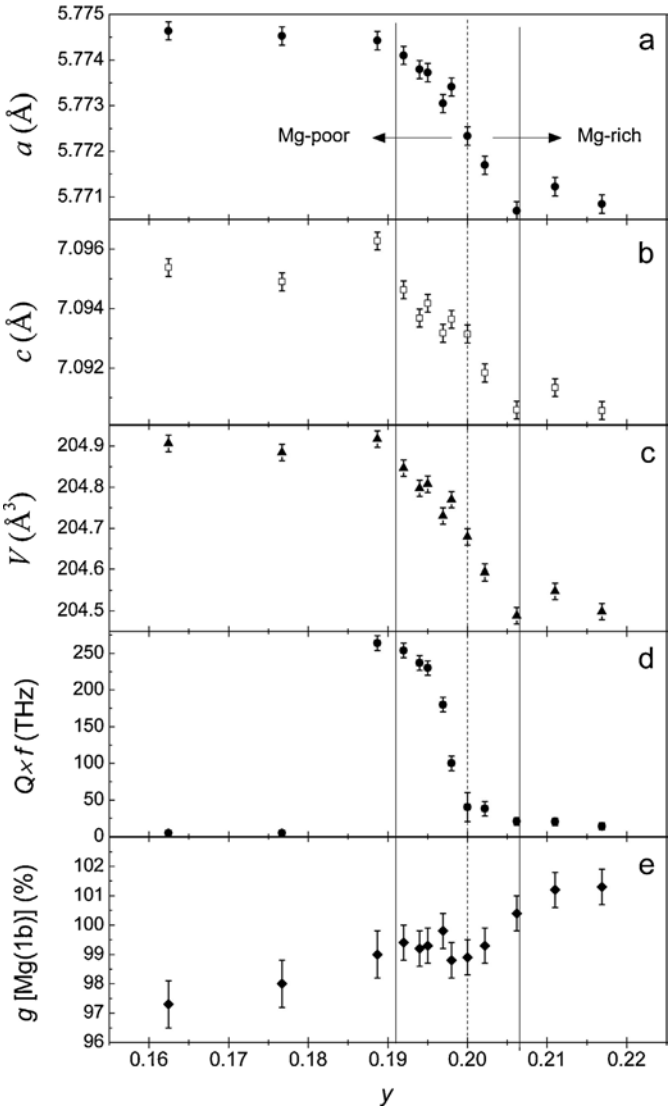

Fig. 4. Evolution of the unit cell parameters a (panel a), c (panel b) and V (panel c) in the off-stoichiometric BMT along the $Mg_4Ta_2O_9$–$Ba_4Ta_2O_9$ tie line. The chemical compositions are expressed by a hypothetical formula: $Ba_{4-5y}Mg_{5y}Ta_2O_9$. The vertical dash line at $y = 0.2$ indicates stoichiometric $BaMg_{1/3}Ta_{2/3}O_3$ composition. Solid lines indicate the limits of the single phase composition. Panel (d) show y dependence of $Q \times f$ and panel (e) shows Mg-site occupancy by Mg ion, g[Mg(1b)].

Because formation energy of cation Frenkel defects in closed-packed perovskites is high, i.e., 6–8 eV per defect,[57] these defects are excluded from further discussion. This leaves two possible mechanisms for accommodation of Mg excess (Ba deficiency) in the BMT along the $Mg_4Ta_2O_9$–$Ba_4Ta_2O_9$ joint. The first mechanism involves vacancy formation where Mg excess (Ba deficiency) along the BMT–$Mg_4Ta_2O_9$ tie line is accommodated by the Ba- and oxygen vacancy complex, $[V''_{Ba}–V_O^{\cdot\cdot}]$, according to: $(Ba_{1-x}V''_{Ba\,x})Mg_{1/3}Ta_{2/3}O_{3-x}V_O^{\cdot\cdot}{}_x$. By analogy, Mg deficiency along the BMT–$Ba_4Ta_2O_9$ joint is accommodated by Mg- and oxygen vacancy complex, $[V''_{Mg}$-$V_O^{\cdot\cdot}]$, according to: $Ba(Mg_{1/3-x}V''_{Mg\,x}Ta_{2/3})O_{3-x}V_O^{\cdot\cdot}{}_x$. In the case of the vacancy compensation mechanism, the unit cell volume is

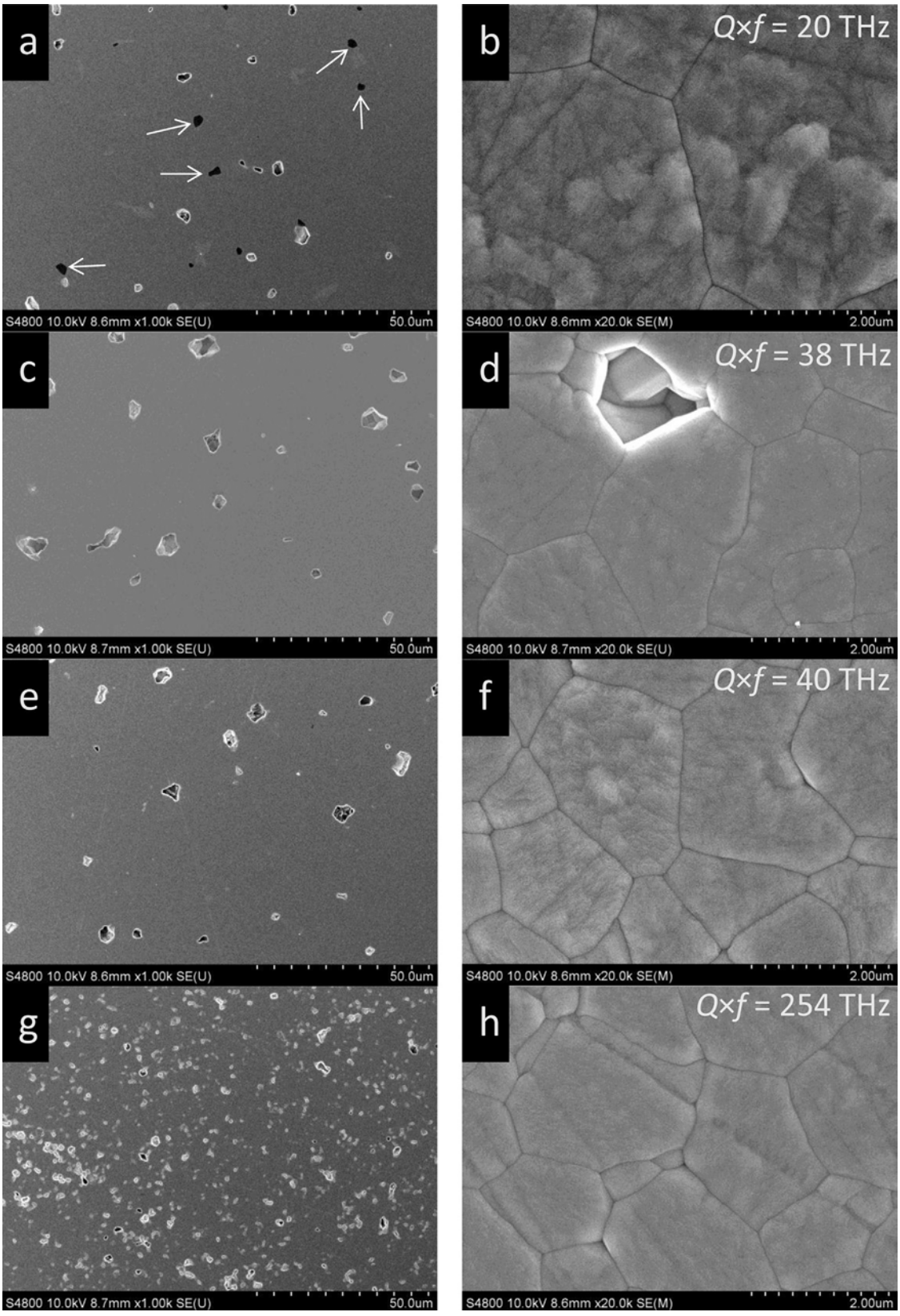

Fig. 5. Scanning electron microscopy images of polished (panels a, c, e, and g), and thermally etched (panels b, d, f, and h) surfaces of $Ba_{4-5y}Mg_{5y}Ta_2O_9$ ceramics along the $Mg_4Ta_2O_9$–$Ba_4Ta_2O_9$ tie line, where $y = 0.211$ (panels a and b), $y = 0.2022$ (panels c and d), $y = 0.2$ (panels e and f), $y = 0.192$ (panels g and h). Please note that Mg-rich BMT ceramics with $y = 0.211$ shows a multi-phase composition. The second phase, $Mg_4Ta_2O_9$, is marked by white arrows. Also note a slight compositional dependence of the grain size. The average grain size decreases with the decrease in Mg concentration along the $Mg_4Ta_2O_9$–$Ba_4Ta_2O_9$ tie line. For detailed crystal and dielectric data of these ceramics please refer to Fig. 4. Ceramics were sintered at 1650 °C for 20 h.

expected to shrink upon deviation from stoichiometry as the lattice accommodates increasing concentration of vacancies. While this scenario may explain the lattice contraction along the BMT–$Mg_4Ta_2O_9$ tie line, it cannot explain a unit cell expansion in the Mg-deficient BMT compounds shown in Fig. 4c. Therefore, in addition to the vacancy model, one needs to consider a 'misplaced ion' mechanism where the excess of Ba or Mg cations enters the alien lattice cites in the form of the Ba_{Mg} or Mg_{Ba} defects, respectively. Notably, this mechanism was first proposed by Desu and O'Bryan to explain an enhancement in the *c*/*a* ratio and an increase in the *Q*-factor found in the $BaZn_{1/3}Ta_{2/3}O_3$ upon partial evaporation of ZnO.[64]

According to a misplaced ion mechanism, the excess Mg along the BMT–$Mg_4Ta_2O_9$ joint is accommodated at the Ba-site as: $(Ba_{1-x}Mg_{Ba\,x})Mg_{1/3}Ta_{2/3}O_3$. Similarly, excess Ba enters Mg site along the BMT–$Ba_4Ta_2O_9$ tie line according to: $Ba(Ba_{Mg\,x}Mg_{1/3-x}Ta_{2/3})O_3$. The defect model based on misplaced ion scenario offers a reasonable account of the experimental data. Indeed, incorporation of a much larger Ba ion on Mg site results in expansion of the unit cell, whereas partial solubility of a small Mg ion in dodecahedral Ba cite produces contraction of the unit cell as supported by the chemical composition dependence of *a*, *c* and *V* shown in Fig. 4a–c. Because Mg^{2+} and Ba^{2+} are isovalent ions, the charge is balanced and no additional cation or anion vacancy is needed during formation of the Ba_{Mg} and Mg_{Ba} defects.

It appears that the crystal lattice arguments alone cannot distinguish between the vacancy and misplaced ion models in Mg-rich BMT because both $[V''_{Ba}\text{-}V_O^{\cdot\cdot}]$ and Mg_{Ba} defects can qualitatively explain the lattice contraction along the BMT–$Mg_4Ta_2O_9$ tie line. It is also from the statistical thermodynamics perspective that both vacancy- and misplaced ion defects must form in $Ba(B'_{1/3}B''_{2/3})O_3$. The question is: Which type of these two defects is the dominant one and how to identify these defects by experimental techniques? These questions are addressed in the following section.

3.4. Origin of extrinsic dielectric loss in single-phase BMT

Analysis of the data in Table 1 as well as Figs. 1 and 4 indicates that the $Q \times f$ value varies from 20 THz to 340 THz for samples that fall within a single-phase BMT composition range. This behavior is puzzling, especially considering an apparent absence of correlation between the 1:2 cation order and the *Q*-factor (see, for example Fig. 4e). Here the author takes an opportunity to put forth a model of extrinsic dielectric loss that explains a large compositional variation of the $Q \times f$ value within a single-phase, 1:2 ordered BMT region.

Both types of defects, $[V''_{Ba}\text{-}V_O^{\cdot\cdot}]$ and Mg_{Ba}, if present, will affect dielectric properties of Mg-rich BMT ceramics, however, their 'dielectric footprint' must be different. By definition, the $[V''_{Ba}\text{-}V_O^{\cdot\cdot}]$ defect complex carries an electric dipole. When subjected to an ac electric field, the dielectric relaxation of this dipole will be determined by the motion of the oxygen vacancy around the immobile V''_{Ba} defect. Some information about the $V_O^{\cdot\cdot}$ dynamics in perovskites can be found in literature. For example, electron paramagnetic resonance study of the alignment of the $V_O^{\cdot\cdot}\text{-}Fe^{3+}$ defect in $BaTiO_3$ under the high electric field reveals that the activation energy for $V_O^{\cdot\cdot}$ hopping between oxygen octahedral sites is 0.91 eV.[65] Because the $V_O^{\cdot\cdot}$ hopping involves phonon-assisted transfer of oxygen ion from one lattice cite to the neighbor vacant site along the edge of the oxygen octahedron, qualitatively similar hopping mechanism of $V_O^{\cdot\cdot}$ between 12 equivalent oxygen sites associated with the $[V''_{Ba}\text{-}V_O^{\cdot\cdot}]$ defect complex would be expected in BMT.

For those working on the $Ba(B'_{1/3}B''_{2/3})O_3$ perovskites, the idea of the Mg_{Ba} defect may look somewhat new because of the large size difference between Mg and Ba ions. Indeed, to the author's knowledge, the possibility of a B'_{Ba} defect in the $Ba(B'_{1/3}B''_{2/3})O_3$ perovskites has never been addressed. Nevertheless, incorporation of much smaller ions into a large lattice sites in ionic crystals is well-documented. The low-temperature physics of the small impurity ions accommodated at large cation or anion sites in the alkali halides has generated a lot of groundbreaking research in the second half of the last century.[66,67] These findings paved the way for latter studies of small substitutional ions in perovskites which invigorated research on dipolar glass and relaxor ferroelectrics. For an excellent review on this topic please see Ref. 68

A relevant example to the Mg-rich BMT case is partial substitution of a small Li ion for a large potassium site in $K_{1-x}Li_xTaO_3$ perovskite studied by nuclear magnetic resonance and dielectric spectroscopy.[69,70] The VI CN Li^+ radius is 0.76 Å and the XII CN K^+ radius is 1.64 Å.[71] These compare quite well with the VI CN Mg^{2+} radius of 0.72 Å and the XII CN Ba^{2+} radius of 1.61 Å.[71] Another relevant example is partial substitution of small divalent ions for Sr-site in $SrTiO_3$. First-principles calculations followed by electron paramagnetic resonance (EPR), dielectric spectroscopy, and X-ray absorption fine structure studies have confirmed substitution of small divalent ions, such as Mg^{2+}, Mn^{2+} and Zn^{2+} for Sr-site in $SrTiO_3$ perovskite.[72–78] A common feature of all these substitutional defects is the low-symmetry ground state associated with the small shift of the ion defect from the center of the dodecahedral perovskite site.[74,75,77,78]

Because of the small size, the short-range repulsive forces acting on the Mg_{Ba} will be dramatically reduced and the (lattice) potential energy of the defect will have a large anharmonic contribution. These are ideal conditions to cause a highly asymmetric equilibrium configuration of the Mg_{Ba} defect. The central idea of the model is that the Mg ion will be located slightly off-center from the dodecahedral position, as outlined schematically in Fig. 6. The exact location and the number of the energy minima of the Mg_{Ba} defect will depend on a delicate balance between the short-range repulsive and long-range polarization forces. Most plausible configuration may involve energy surface having 6 potential minima in the ⟨10 0⟩ directions of the ideal cubic perovskite cell. This type of the ground state shown in Fig. 6 has been found, for example, in $Sr_{1-x}Mg_xTiO_3$, $Sr_{1-x}Mn_xTiO_3$, $Sr_{1-x}Zn_xTiO_3$, and $K_{1-x}Li_xTaO_3$.[69,74] Another plausible configuration is described by the 12-valley energy minima (not shown) with Mg^{2+} ion shifted in the ⟨110⟩ directions toward one of the 12 equidistant oxygens. This type of potential energy surface has been reported, for example, in $Li_xK_{1-x}Cl$.[66]

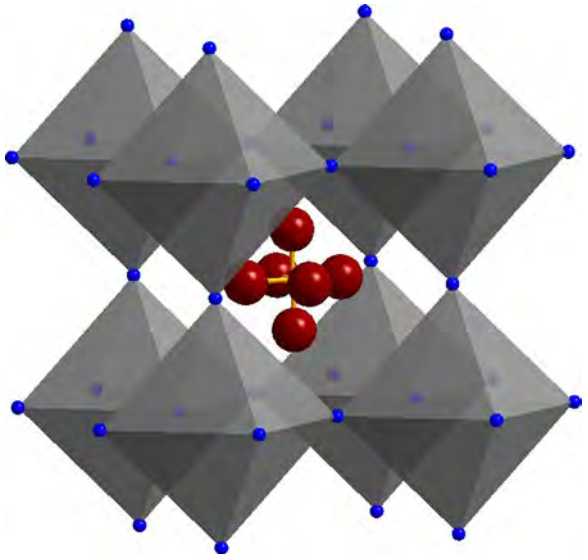

Fig. 6. Proposed schematic of the Mg_{Ba} defect. Here Mg^{2+} ion (red sphere) is shifted from the center of the Ba dodecahedral cite along 6 equiv. ⟨1 0 0⟩ directions of the ideal cubic perovskite cell. Oxygen ions are represented by small blue spheres. The rest of the ions are omitted for clarity. The 'rattling' of Mg_{Ba} defect is a source of extrinsic dielectric loss in BMT. In the figure, the off-center Mg displacement amplitude is exaggerated for clarity and the ionic radii are not to scale. (For interpretation of the references to color in this figure legend, the reader is referred to the web version of the article.)

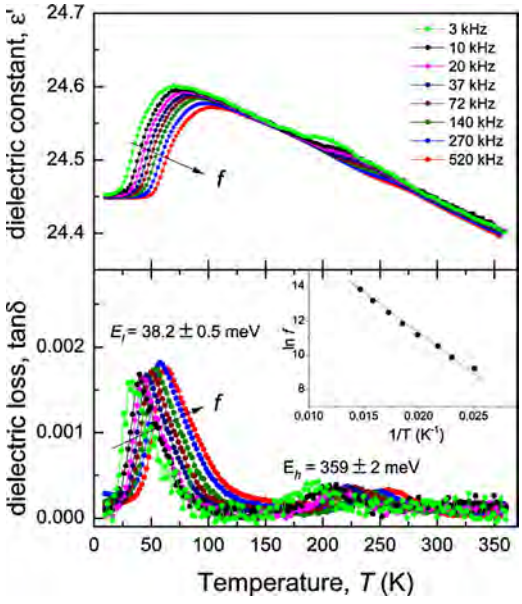

Fig. 7. Dielectric properties of Mg-rich BMT sample C6 measured at f = 3, 10, 20, 37, 72, 140, 270 and 520 kHz. The sample target composition is given in Table 1. Arrows indicate increasing frequency. Activation energies for low- and high-temperature relaxation processes are indicated by E_l and E_h, respectively. As a way of example, the inset shows the low-energy (E_l = 38.2 meV) dielectric relaxation fit to Eq. (3).

Unlike Mn^{2+} ion, whose lattice position can be determined by a local probe, such as EPR, the Mg^{2+} has no unpaired spins and therefore it is EPR-silent. Concerning a nuclear magnetic resonance (NMR), which is also an excellent local symmetry probe for atoms with non-zero nuclear spin, it is challenging to detect Mg because ^{25}Mg spin 5/2 nucleus is quadrupolar. The NMR signal width increases with asymmetry and therefore detecting asymmetric Mg_{Ba} defect in relatively small concentrations will be extremely challenging if not impossible. In other words, the author is not aware of any direct local probe method for detection of the Mg_{Ba} defect in BMT. Among the indirect methods, dielectric spectroscopy is the most sensitive technique for detection of small point defect concentrations. If the proposed model is correct and Mg_{Ba} defect is off-centered in BMT it will carry an electric dipole moment which can be probed by dielectric spectroscopy. It is expected then that Mg_{Ba} will 'rattle' between the equivalent off-center sites either by direct tunneling[67] or by phonon-assisted hopping.[68] Dielectric spectroscopy has been extensively used in the past to study dipolar dynamics and providing an indirect evidence of, for example, Mg_{Sr} and Mn_{Sr} defects in $SrTiO_3$.[73,75,76] The low-frequency dielectric spectroscopy is used in this study to probe the dynamics of both the $[V''_{Ba}\text{-}V_O^{\cdot\cdot}]$ and Mg_{Ba} defects in BMT.

Fig. 7 shows the low-frequency dielectric data (ε' and tan δ) of Mg-rich BMT sample (sample C6, Table 1) measured in the 10–350 K interval. The frequency-dependent low-temperature peak at 70 K and high-temperature shoulder at 200 K in the ε' data indicate that there are two different relaxation mechanisms. The activation energy, E_i, of the dielectric relaxation process was extracted from the Arrhenius plot of the frequency-dependent tanδ peaks,

$$f = f_0 \, exp\left(-\frac{E_i}{k_B T_{max}}\right), \quad (3)$$

where T_{max} is a temperature of the tan δ maximum at frequency f.

The linear fit to Eq. (3) (shown in the inset in Fig. 7) yields E_l = 38.2 ± 0.5 meV and E_h = 359 ± 2 meV for low- and high-temperature dielectric relaxations, respectively. Both low- and high-temperature features are absent in the dielectric data of Mg-deficient BMT (sample G63, Table 1) shown in Fig. 8. The dielectric relaxation process with E_l = 38.2 ± 0.5 meV is assigned to the rattling of the Mg_{Ba} defects in Mg-rich BMT. It indicates that there exist a low-energy path between the equivalent off-center Mg positions in the dodecahedral cite of BMT lattice. The activation energy of 38.2 meV for Mg_{Ba} is in good agreement with an activation energy of 31 meV reported for dielectric relaxation of Mg_{Sr} defect in $Sr_{1-x}Mg_xTiO_3$.[73] The volume of the dodecahedral site in BMT is slightly larger than that in $SrTiO_3$. This may explain somewhat stronger off-center localization of the Mg_{Ba} defect in BMT as compared with the Mg_{Sr} in $Sr_{1-x}Mg_xTiO_3$. Both the experimental energies are in fair agreement with the value of 18.5 meV for Mg_{Sr} potential well found by the first-principles calculations.[74]

Next, we tentatively assign the high-temperature ε' shoulder in Fig. 7 with E_h = 359 ± 2 meV to the dielectric relaxation associated with the $[V''_{Ba}\text{-}V_O^{\cdot\cdot}]$ dipolar defect, although the activation energy is noticeably lower than the 910 meV and 640 meV reported for oxygen vacancy relaxation in $BaTiO_3$ and $SrTiO_3$, respectively.[65,79] From the relative intensity of the low- and

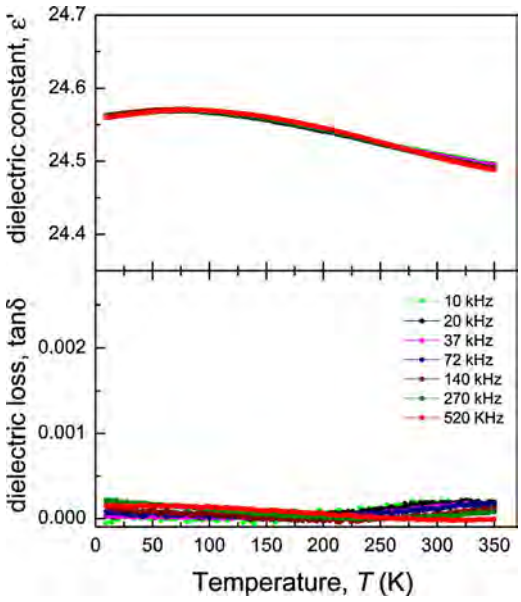

Fig. 8. Dielectric properties of Mg-poor BMT sample G63. The target composition of the sample is given in Table 1. The data are plotted at the same scale as in Fig. 7.

high-temperature tan δ peaks in Fig. 7 it is clear that the Mg_{Ba} is a dominant defect in Mg-rich BMT, although more detailed analysis of the dipolar moments of both $[V_{Ba}^{''}\text{-}V_{O}^{\cdot\cdot}]$ and Mg_{Ba} defects is required for more accurate comparison of their relative concentrations. In contrast to the 'rattling' Mg_{Ba} defect, misplaced Ba_{Mg} does not cause Debye-type dielectric loss because the motion of the large Ba^{2+} ion located at the Mg site is tightly arrested by the oxygen ligands. This rationale is supported by the absence of dielectric anomalies in the Mg-deficient BMT sample (see Fig. 8).

In addition to the direct contribution to the tan δ, dielectric relaxation of both the $[V_{Ba}^{''}\text{-}V_{O}^{\cdot\cdot}]$ and Mg_{Ba}-induced dipoles occurs by (multi)phonon assisted hopping and therefore will affect the phonon lifetimes and damping constant of atomic vibrations in BMT.[80,81] It can be reasonably argued that due to the large difference in the ionic radii, the formation energy of the Mg_{Ba} and Ba_{Mg} defects, and their equilibrium concentrations at a given temperature, must be quite different. We leave the thermodynamics of the misplaced ion defects in BMT for future studies. At this stage, our experimental results demonstrate that by reducing chemical activity of Mg in BMT, one can shift the defect equilibrium from Mg_{Ba}-dominated defects to Ba_{Mg}-dominated defects. This simple method proves to be very effective in reducing extrinsic dielectric loss in BMT ceramics. Upon further optimization of processing conditions, this method yields BMT with $Q \times f \approx 380$–390 THz.[82]

3.5. Effect of atomic order and lattice distortion on dielectric loss

The role of the 1:2 cation order in the dielectric loss of $Ba(B'_{1/3}B''_{2/3})O_3$ ceramics has been addressed in early literature with rather conflicting conclusions. Several papers attribute the high $Q \times f$ values to the high degree of 1:2 order in BZT and BMT ceramics.[64,83,84] At the same time, very high $Q \times f$ values in completely disordered BZT- and BMT-based ceramics were reported by other authors.[19,85,86] Finally, Koga et al.,[29] reported that both high and low $Q \times f$ values are found in ordered BZT emphasizing that the 1:2 order alone is insufficient for obtaining high-Q ceramics. The author's results on BMT presented herein are in line with the latter findings.

In most cases studied here, the B-site occupancies have refined to the values close to unity indicating completely ordered structure. However, the non-stoichiometric Ta-poor and Ba-rich BMT samples located in D and E CTs had significant degree of disorder with very broad $\pm 1/3\{hkl\}$ supercell reflections due to a small size of the 1:2 ordered domains. These latter cases were rather difficult to refine using a single histogram approach because of the very different peak profiles for sub- and supercell reflections. For these particular cases an additional 'brute force' method was used to achieve a more accurate estimate of the cation occupancy. First, the ordering parameter, S, was deduced from the ratio of the X-ray integrated intensity of the strongest suppercell peak, (1 0 0), to the integrated intensity of the strongest peak of the BMT structure, (1 1 0). With laboratory X-rays, the (0 1 2) and (1 0 2) peaks are very close to (1 1 0), therefore, they also were taken into account in the calculations. The ordering parameter is given by

$$S = \sqrt{\frac{(I_{100}/I_{110,012,102})_{obs}}{(I_{100}/I_{110,012,102})_{calc}}}, \quad (4)$$

where $(I_{100}/I_{110,012,102})_{obs}$ is the ratio of the observed integrated intensity of the (1 0 0) supercell reflection to that of (1 1 0, 0 1 2, 1 0 2) main reflection, and $(I_{100}/I_{110,012,102})_{calc} = 0.0827$ is the calculated value for a completely ordered BMT structure.[87] Second, the g[Mg(1b)] cation occupancy was calculated assuming that the complete B-site cation disorder ($S = 0$) corresponds to the 33.3% of Mg(1b) sites occupied by Mg ions and remaining 66.6% occupied by Ta ions.[36]

An example of Rietveld profile refinement for single-phase BMT sample C6 with $Q \times f = 21$ THz having high degree of 1:2 cation ordering is shown in Fig. 9. The refined structural parameters of C6 ($Q \times f = 21$ THz) and H61 ($Q \times f = 330$ THz) samples as well as partially disordered D16 sample are listed in Table 2, while their chemical composition and dielectric properties are given in Table 1. Note that both C6 and H61 samples show nearly identical partial occupancies of the Mg(1b) and Ta(2d) sites indicating complete 1:2 cation order.

In contrast, Ta-deficient and Ba-rich D16 sample shows substantial degree of disorder with 18.7% of Mg-sites occupied by Ta ions (Table 2). It appears that (partial) B-site cation disorder in Ba-rich and Ta/Nb-deficient $Ba(B'_{1/3}B''_{2/3})O_3$ perovskites is rather common phenomenon reported for BZT, BZN and BMT.[29,30,88–90] Our results of atomic order in BMT are at variance with those reported by Surendran et al.[27] The authors of Ref. 27 found that both stoichiometric and non-stoichiometric BMT samples demonstrate significant degree of atomic disorder (e.g., $S < 80\,\%$). The reason for high degree of atomic disorder in the BMT samples studied in Ref. 27 is unknown to the author. It is only speculated here that the use of the

Table 2
Refined structural parameters, fractional site occupancies, selected interatomic distances, reliability factors for BMT samples C6, H61 and D16 with target chemical compositions given in Table 1. The structure was refined within the $P\bar{3}m1$ space group, No. 164, with atomic fractional coordinate positions of Ba1(1a)[0, 0, 0], Ba2(2d)[1/3, 2/3, z] with $z \approx 2/3$, Mg(1b)[0, 0, 1/2], Ta(2d)[1/3, 2/3, z] with $z \approx 1/6$, O1(3e)[1/2, 0, 0], O2(6i)[x, 2x, z] with $x \approx 1/6$ and $z \approx 1/3$.

	C6	H61	D16
$Q \times f$ (THz)	21	330	Undefined
a (Å)	5.77201(5)	5.77443(9)	5.7785(2)
c (Å)	7.09222(6)	7.0973(12)	7.0865(3)
c/a	1.2287	1.2291	1.2264
Ba2 z	0.6636(3)	0.6650(3)	0.6648(4)
Ta z	0.1775(2)	0.1765(2)	0.1740(3)
O2 x	0.1689(8)	0.1697(7)	0.1727(9)
O2 z	0.331(12)	0.318(11)	0.338(14)
g(Mg)/g(Ta) (site 1b)	1.0052(3)/−0.0052(3)	1.0033(3)/−0.0033(3)	0.813(9)/0.187(9)
g(Ta)/g(Mg) (site 2d)	1.0026(3)/−0.0026(3)	1.0016(3)/−0.0016(3)	0.906(9)/0.094(9)
×6 Ba1–O1 (Å)	2.8859(9)	2.8872(9)	2.8892(1)
×6 Ba1–O2 (Å)	2.898(8)	2.823(8)	2.953(9)
×3 Ba2–O1 (Å)	2.909(2)	2.904(15)	2.903(3)
×3 Ba2–O2 (Å)	2.869(8)	2.959(8)	2.819(9)
×6 Ba2–O2 (Å)	2.8862(1)	2.8899(4)	2.8899(2)
×3 Ta–O1 (Å)	2.089(10)	2.0852(9)	2.075(15)
×3 Ta–O2 (Å)	1.972(8)	1.919(7)	1.98(11)
×6 Mg–O2 (Å)	2.070(8)	2.134(7)	2.08(10)
R_p (%)	8.06	7.86	9.67
R_{wp} (%)	11.16	10.61	14.21
GOF	2.34	2.12	2.97

hydrous $(MgCO_3)_4 \cdot Mg(OH)_2 \cdot 5H_2O$ precursor in Ref. 27 may have caused unexpected deviation from the targeted sample stoichiometry.

While more detailed analysis of the structural parameters of the non-stoichiometric BMT and their possible correlation with dielectric properties will be published elsewhere, the author would like to emphasize here several interesting trends. It is well known that the 1:2 cation ordering causes an increase in the trigonal lattice distortion, i.e., the c/a lattice parameter ratio deviates from the $\sqrt{3/2} = 1.2247$ value for the ideal cubic structure. It is somewhat puzzling that the data in Tables 1 and 2 show large variation of the c/a ratio even for samples having very similar degree of the 1:2 cation order. Over the course of this study it became clear that the BMT ceramics with $c/a \geq 1.2291$ always show high Q-factors (e.g., $Q \times f \geq 280$ THz), provided ceramics are single-phase (see Table 1). Another peculiar observation concerns the Ta–O and Mg–O bond lengths. Because BMT has a tolerance factor slightly larger than unity, Ba ions are over-bonded, i.e., they are under compression stress, whereas B-site cations are under-bonded, i.e., they experience tensile environment of the oxygen octahedra.[91] This, together with electrostatic forces induced by 1:2 ordering, causes Ta ions to shift from the center of the TaO_6 octahedra toward the layer of the neighboring MgO_6. Remarkably, off-center distortion of the Ta ions is the largest in the high-Q BMT as evidenced by the large difference in the bond lengths of Ta–O1 = 2.0852(9) Å ×3 and Ta–O2 = 1.919(7) Å ×3 (sample H61 in Table 2).

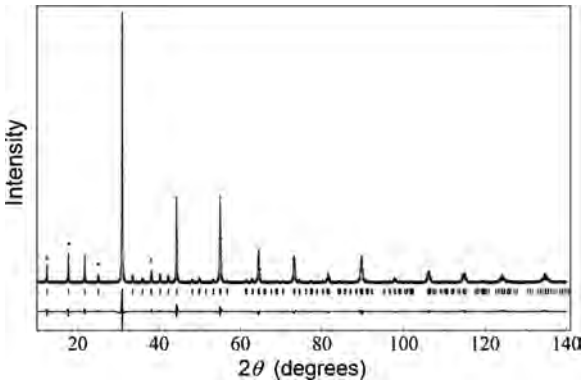

Fig. 9. Room temperature X-ray diffraction pattern (+) of single-phase sample C6 with $Q \times f = 21$ THz. Calculated diffraction pattern from Rietveld refinement ($P\bar{3}m1$ space group) is shown by solid line. The vertical bars indicate the positions of expected Bragg peaks. Major peaks associated with the 1:2 cation order are marked by asterisk. The difference between observed and calculated data is shown at the bottom of the plot. Structural details of refinement are given in Table 2.

Desu and O'Bryan[64] attributed a gradual increase in the c/a ratio in completely ordered high-Q BZT to a partial incorporation of Ba ions into the Zn-sites due to Zn evaporation at high temperatures. It seems that this model can also explain an increase in the c/a ratio in the Mg-deficient BMT reported here due to partial accommodation of Ba at Mg-sublattice. Replacement of Mg by Ba will also cause an expansion of the MgO_6 octahedra. This is consistent with an increase in the Mg–O2 bond length observed in Mg-deficient sample H61 with Mg–O2 = 2.134(7) Å ×6 as compared to 2.070(8) Å ×6 for Mg-rich sample C6 (see Table 2).

4. Concluding remarks

Dielectric loss in $BaMg_{1/3}Ta_{2/3}O_3$ perovskite ceramics strongly depend on small changes in the chemical composition. Completely ordered, dense, single-phase BMT ceramics

sintered at 1650 °C for 20 h show $Q \times f$ variation in the range of 20–340 THz. It is demonstrated, therefore, that in the case of BMT ceramics, complete 1:2 cation order on the B-site is insufficient to achieve the high-Q microwave dielectric resonators. The dominant source of the extrinsic dielectric loss in BMT is identified as Mg_{Ba} defect 'rattling' inside the dodecahedral Ba position. The simplest way to minimize the extrinsic dielectric loss is to reduce the chemical potential of Mg ion in BMT by shifting the chemical composition toward the Mg-deficient region. Without the use of any dopants or 'sintering aids', this method brings a significant enhancement in the Q-factor of the $BaMg_{1/3}Ta_{2/3}O_3$ ceramics. It is obvious that the proposed approach is quite general in a way that it can be used to suppress the possible B'_{Ba} defects and accompanying extrinsic dielectric loss in other technically important $Ba(B'_{1/3}B''_{2/3})O_3$ perovskites.

Acknowledgements

This work was supported by JSPS Grant-in-Aid for Scientific Research C 21560025. The author is indebted to Alexei A. Belik for his assistance with Rietveld refinement using RIETAN 2000. The author also thanks R&D staff of Com. Dev. Int. including Ming Yu, William Fitzpatrick and Antonio Panariello for their continuous technical advise and interest in this work.

References

1. Galasso F, Pyle J. Ordering in compounds of $A(B'_{0.33}B''_{0.67})O_3$ type. *Inorg Chem* 1963;**2**:482–4.
2. Galasso F, Barrante JR, Katz L. Alkaline earth tantalum oxygen phases including the crystal structure of an ordered perovskite compound, $Ba_3SrTa_2O_9$. *J Am Chem Soc* 1961;**83**:2830–2.
3. Sagala DA, Nambu S. Lattice energy calculations for ordered and disordered $BaZn_{1/3}Ta_{2/3}O_3$. *J Phys Soc Jpn* 1992;**61**:1791–7.
4. Bellaiche L, Vanderbilt D. Electrostatic model of atomic ordering in complex perovskite alloys. *Phys Rev Lett* 1998;**81**:1318–21.
5. Bellaiche L, Padilla J, Vanderbilt D. Heterovalent and A-atom effects in $A(B'B'')O_3$ perovskite alloys. *Phys Rev B* 1999;**59**:1834–9.
6. Burton BP. Empirical cluster expansion models of cation order-disorder in $A(B'_{1/3}B''_{2/3})O_3$ perovskites. *Phys Rev B* 1999;**59**:6087–91.
7. Burton BP, Cockayne E. Why $Pb(BB')O_3$ perovskites disorder at lower temperatures than $Ba(BB')O_3$ perovskites? *Phys Rev B* 1999;**60**:R12542–5.
8. Takahashi T. First-principles investigation of the phase stability for $Ba(B'2+_{1/3}B''5+_{2/3})O_3$ microwave dielectrics with the complex perovskite structure. *Jpn J Appl Phys* 2000;**39**:5637–41.
9. Nomura S, Toyama K, Kaneta K. $BaMg_{1/3}Ta_{2/3}O_3$ ceramics with temperature-stable high dielectric constant and low microwave loss. *Jpn J Appl Phys* 1982;**21**:L624–6.
10. Fiedziuszko SJ, Hunter IC, Itoh T, Kobayashi Y, Nishikawa T, Stitzer SN, et al. Dielectric materials, devices and circuits. *IEEE Trans Microwave Theory Tech* 2002;**50**:706–20.
11. Kolodiazhnyi T, Annino G, Shimada T. Intrinsic limit of dielectric loss in several $Ba(B'_{1/3}B''_{2/3})O_3$ ceramics revealed by the whispering-gallery mode technique. *Appl Phys Lett* 2005;**87**:212908.
12. Petzelt J, Setter N. Far infrared spectroscopy and origin of microwave losses in low-loss ceramics. *Ferroelectrics* 1993;**150**:89–102.
13. Petzelt J, Kamba S, Kozlov GV, Volkov AA. Dielectric properties of microwave ceramics investigated by infrared and submillimeter spectroscopy. *Ferroelectrics* 1996;**176**:145–65.
14. Konoike T, Tamura H. United States Patent 4,585,744.
15. Nomura S, Konishi Y. United States Patent 4,487,842.
16. Sugiyama M, Inuzuka T, Kubo H. United States Patent 5,057,466.
17. Yokoi H, Tosa A, Ohbayashi K. United States Patent 6,117,806.
18. Shimada T, Nishikawa K, Toji K. United States Patent 6,331,498 B1.
19. Matsumoto H, Tamura H, Wakino K. $Ba(Mg,Ta)O_3$–$BaSnO_3$ high-Q dielectric resonator. *Jpn J Appl Phys* 1991;**30**:2347–9.
20. Furuya M, Ochi A. Microwave dielectric properties for $BaMg_{1/3}Ta_{2/3}O_3$–$A(Mg_{1/2}W_{1/2})O_3$ (A = Ba, Sr, Ca) ceramics. *Jpn J Appl Phys* 1994;**33**:5482–7.
21. Chai L, Akbas MA, Davies PK, Parise JP. Cation ordering transformations in $BaMg_{1/3}Ta_{2/3}O_3$–$BaZrO_3$ solid solutions. *Mater Res Bull* 1997;**32**:1261–9.
22. Chai L, Davies PK. Effect of M^{4+} (Ce, Sn, Ti) B-site substitutions on the cation ordering in $BaMg_{1/3}Ta_{2/3}O_3$. *Mater Res Bull* 1998;**33**:1283–92.
23. Sugiyama M, Inuzuka T, Kubo H. Effects of processing on microstructure and dielectric properties in barium magnesium tantalum oxide ($Ba(Mg_{1/3}Ta_{2/3})O_3$) ceramics. *Ceram Trans* 1990;**15**:153–6.
24. Youn H-J, Kim K-Y, Kim H. Microstructural characteristics of $BaMg_{1/3}Ta_{2/3}O_3$ ceramics and its related microwave dielectric properties. *Jpn J Appl Phys* 1996;**35**:3947–53.
25. Kolodiazhnyi T, Petric A, Johari G, Belous AG. Effect of preparation conditions on cation ordering and dielectric properties of $Ba(Mg_{1/3}Ta_{2/3})O_3$ ceramics. *J Eur Ceram Soc* 2002;**22**:2013–21.
26. Fujimaru T, Nishida M, Kugimiya K. United States Patent 5,246,898.
27. Surendran KP, Sebastian MT, Mohanan P, Moreira RL, Dias A. Effect of nonstoichiometry on the structure and microwave dielectric properties of $Ba(Mg_{0.33}Ta_{0.67})O_3$. *Chem Mater* 2005;**17**:142–51, and references therein.
28. Koga E, Moriwake H, Kakimoto K, Ohsato H. Influences of composition deviation from stoichiometric $BaZn_{1/3}Ta_{2/3}O_3$ on superlattice ordering and microwave quality factor Q. *J Ceram Soc Jpn* 2005;**113**:172–8.
29. Koga E, Yamagishi Y, Moriwake H, Kakimoto K, Ohsato H. Large Q factor variation within dense, highly ordered $Ba(Zn_{1/3}Ta_{2/3})O_3$ system. *J Eur Ceram Soc* 2006;**26**:1961–4.
30. Wu H, Davies PK. Influence of non-stoichiometry on the structure and properties of $BaZn_{1/3}Nb_{2/3}O_3$ microwave dielectrics. II: Compositional variations in pure BZN. *J Am Ceram Soc* 2006;**89**:2250–63.
31. Paik JH, Nahm S, Bylin JD, Kim MH, Lee HJ. The effect of Mg defficiency on the microwave dielectric properties of $BaMg_{1/3}Nb_{2/3}O_3$ ceramics. *J Mater Sci Lett* 1998;**17**:1777–80.
32. Ovchar O, Durylin D, Belous A, Jancar B, Kolodiazhnyi T. A-site deficient perovskites $Ba(M^{2+}_{1/3}Nb_{2/3})O_3$: microstructural attributes for a high quality factor. *Mater Sci Poland* 2011;**29**:56–62.
33. Belous AG, Ovchar OV, Kramarenko AV, Jancar B, Bezjak J, Suvorov D. Effect of nonstoichiometry on the structure and microwave dielectric properties of $BaCo_{1/3}Nb_{2/3}O_3$. *Inorg Mater* 2010;**46**:529–33.
34. Yamagiwa K, Otsuka J, Kasashima T, Sato M, Itakura K, Oba T, et al. United States Patent 6,720,280 B2.
35. Izumi F, Ikeda T. A Rietveld-analysis program RIETAN-98 and its applications to zeolites. *Mater Sci Forum* 2000;**321–324**:198–205.
36. Vincent H, Perrier Ch, l'Heritier Ph, Labeyrie M. Crystallographic study, by Rietveld's method, of barium–magnesium–tantalum oxides based ceramics for use as dielectric resonator. X-ray dilatometry at low temperature. *Mater Res Bull* 1993;**28**:951–8.
37. http://www.qwed.eu/
38. Kolodiazhnyi T, Sakurai H, Vittayakorn N. Spin-flop driven magnetodielectric effect in $Co_4Nb_2O_9$. *Appl Phys Lett* 2011;**99**:132906.
39. Kolodiazhnyi T, Belik AA, Ozawa TC, Takayama-Muromachi E. Phase equilibria in the BaO–MgO–Ta_2O_5 system. *J Mater Chem* 2009;**19**:8212–5, and references therein.
40. Kryshtop VG, Devlikanova RU, Filip'ev VS, Fesenko EG. Crystal-chemical conditions for the existence of complex oxides of the $A_6B_{10}O_{30}$ type with tetragonal potassium–tungsten bronze structure. *Inorg Mater* 1983;**19**:945–8.
41. Ovchar O, Durilin D, Belous A, Porokhonskyy V, Jancar B, Kolodiazhnyi T. Tetragonal tungsten bronzes in $Ba(M^{2+}_{1/3}Nb_{2/3})O_3$ microwave ceramics. *Ferroelectrics* 2012;**435**:176–82.
42. Ovchar O, Durylin D, Belous A, Jancar B, Kolodiazhnyi T. Dielectric and relaxor properties of $Ba_9MNb_{14}O_{45}$ ceramics. *J Am Ceram Soc* 2012;**95**:3202–6.

43. Wang L, Sakka Y, Rusakov DA, Mozharivskyj Y, Kolodiazhnyi T. Novel incipient ferroelectrics based on $Ba_4MNb_xTa_{10-x}O_{30}$ where M = Zn, Mg, Co, Ni. *Chem Mater* 2011;**23**:2586–94.
44. Mallinson P, Claridge JB, Iddles D, Price T, Ibberson RM, Allix M, et al. New 10-layer hexagonal perovskites: relationship between cation and vacancy ordering and microwave dielectric loss. *Chem Mater* 2006;**18**: 6227–38.
45. Kovba LM, Lykova LN, Paromova MV, Lopato LM, Shevchenko AV. Barium oxide–tantalum oxide system. *Zh Neorg Khim* 1977;**22**:2845–7.
46. Kovba LM, Lykova LN, Paromova MV, Pol'shchikova ZYa. Polymorphism of barium tantalate $Ba_6Ta_2O_{11}$. *Zh Neorg Khim* 1977;**22**:2584–6.
47. Paramova MV, Leshchenko PP, Lykova LN, Kovba LM. Polymorphism of barium tantalate $Ba_4Ta_2O_9$. *Vestnik Moskovskogo Univ Ser 2: Khim* 1976;**17**:499–501.
48. Ogawa H, Kan A, Ishihara S, Higashida Y. Crystal structure of corundum type $Mg_4(Nb_{2-x}Ta_x)O_9$ microwave dielectric ceramics with low dielectric loss. *J Eur Ceram Soc* 2003;**23**:2485–8.
49. Kan A, Ogawa H, Sumino M, Nishizuka M, Suzuki E. Microwave dielectric properties of xMgO–$(1-x)B_2O_3$ ceramics. *Jpn J Appl Phys* 2009;**48**:09KE03.
50. Kolodiazhnyi T. $BaMg_{1/3}Nb_{2/3}O_3$-$Mg_4Nb_2O_9$ composite microwave ceramics with high Q-factor and low sintering temperature. *J Eur Ceram Soc* 2012;**32**:4305–9.
51. Ohsato H, Koga E, Kagomiya I, Kakimoto K. Dense composition with high Q on the complex perovskite compounds. *Ferroelectrics* 2009;**387**: 28–35.
52. Abe M, Uchino K. X-ray study of the deficient perovskite $La_{2/3}TiO_3$. *Mat Res Bull* 1974;**9**:147–55.
53. Gong W, Yun H, Ning YB, Greedan JE, Datars WR, Stager CV. Oxygen-deficient $SrTiO_{3-x}$, $x = 0.28$, 0.17, and 0.08. Crystal growth, crystal structure, magnetic, and transport properties. *J Solid St Chem* 1991;**90**:320–30.
54. Erhart P, Albe K. Thermodynamics of mono- and di-vacancies in barium titanate. *J Appl Phys* 2007;**102**:084111.
55. Lee S, Liu Z-K, Randall CA. Modified phase diagram for the barium oxide–titanium dioxide system for the ferroelectric barium titanate. *J Am Ceram Soc* 2007;**90**:2589–94.
56. Akhtar MJ, Akhtar Z, Jackson RA, Catlow CRA. Computer simulation studies of strontium titanate. *J Am Ceram Soc* 1995;**78**:421–8.
57. Lewis GV, Catlow CRA. Defect studies of doped and undoped barium titanate using computer simulation techniques. *J Phys Chem Solids* 1986;**47**:89–97.
58. Kuklja MM, Mastrikov YA, Jansang B, Kotomin EA. The intrinsic defects, disordering, and structural stability of $Ba_xSr_{1x}Co_yFe_{1y}O_3$ perovskite solid solutions. *J Phys Chem C* 2012;**116**:18605–11.
59. Wang L, Sakka Y, Shao Y, Botton G, Kolodiazhnyi T. Coexistence of A- and B-site vacancy compensation in La-doped $Sr_{1-x}Ba_xTiO_3$. *J Am Ceram Soc* 2010;**93**:2903–8.
60. Kolodiazhnyi T, Pumera M. Towards ultrasensitive method for determination of metal impurities in carbon nanotubes. *Small* 2008;**4**:1476–84.
61. Valant M, Kolodiazhnyi T, Axelsson A-K, Babu G, Alford NMcN. Spin ordering in Mn-doped $KTaO_3$? *Chem Mater* 2010;**22**:1952–4.
62. Valant M, Kolodiazhnyi T, Arčon I, Aguesse F, Axelsson A-K, Alford NMcN. Response to 'Comment on the origin of magnetism in Mn-doped $SrTiO_3$'. *Adv Funct Mater* 2013;**23**:2231–2.
63. Hui S, Petric A. Electrical properties of yttrium-doped strontium titanate under reducing conditions. *J Electrochem Soc* 2002;**149**:J1–10.
64. Desu SB, O'Bryan HM. Microwave loss quality of $BaZn_{1/3}Ta_{2/3}O_3$ ceramics. *J Am Ceram Soc* 1985;**68**:546–51.
65. Warren WL, Vanheusden K, Dimos D, Pike GE, Tuttle BA. Oxygen vacancy motion in perovskite oxides. *J Am Ceram Soc* 1996;**79**:536–8.
66. Dienes GJ, Hatcher RD, Smoluchowski R, Wilson W. Minimum-energy configuration of Li in KCl. *Phys Rev Lett* 1966;**16**:25–7.
67. Narayanamurti V, Pohl RO. Tunneling states of defects in solids. *Rev Mod Phys* 1970;**42**:201–35.
68. Samara GA. The relaxational properties of compositionally disordered ABO_3 perovskites. *J Phys Condens Matter* 2003;**15**:R367–411, and references therein.
69. Höchli UT, Maglione M. Dielectric relaxation spectroscopy and the ground state of $K_{1-x}Li_xTaO_3$. *J Phys: Condens Matter* 1989;**1**:2241–56.
70. Borsa F, Höchli UT, van der Klink JJ, Rytz D. Condensation of random-site electric dipoles: Li in $KTaO_3$. *Phys Rev Lett* 1980;**45**:1884–7.
71. Shannon RD. Revised effective ionic radii and systematic studies of interatomic distances in halides and chalcogenides. *Acta Crystallogr Sect A* 1976;**32**:751–67.
72. Kvyatkovskii OE. On the nature of ferroelectricity in $Sr_{1x}A_xTiO_3$ and $KTa_{1x}Nb_xO_3$ solid solutions. *Phys Solid State* 2002;**44**:1135–44.
73. Tkach A, Vilarinho PM, Kholkin A. Effect of Mg doping on the structural and dielectric properties of strontium titanate ceramics. *Appl Phys A* 2004;**79**:2013–20.
74. Kvyatkovskii OE. Ab initio study of the on-site potential for divalent impurities in dilute $Sr_{1-x}A_xTiO_3$ solid solutions. *Ferroelectrics* 2005;**314**:143–8.
75. Tkach A, Vilarinho PM, Kholkin AL, Pashkin A, Veljko S, Petzelt J. Broadband dielectric spectroscopy analysis of relaxational dynamics in Mn-doped $SrTiO_3$ ceramics. *Phys Rev B* 2006;**73**:104113.
76. Tkach A, Vilarinho PM, Kholkin AL. Dependence of dielectric properties of manganese-doped strontium titanate ceramics on sintering atmosphere. *Acta Mater* 2006;**54**:5385–91.
77. Laguta VV, Kondakova IV, Bykov IP, Glinchuk MD, Tkach A, Vilarinho PM, et al. Electron spin resonance investigation of Mn^{2+} ions and their dynamics in Mn-doped $SrTiO_3$. *Phys Rev B* 2007;**76**:054104.
78. Levin I, Krayzman V, Woicik JC, Tkach A, Vilarinho PM. X-ray absorption fine structure studies of Mn coordination in doped perovskite $SrTiO_3$. *Appl Phys Lett* 2010;**96**:052904.
79. Wang CC, Lei CM, Wang GJ, Sun XH, Li T, Huang SG, Wang H, Li YD. Oxygen-vacancy-related dielectric relaxations in $SrTiO_3$ at high temperatures. *J Appl Phys* 2013;**113**:094103.
80. Shimada T, Touji K, Liu H-L, Tzeng I-T, Chia C-T, Kolodiazhnyi T. Signature of lattice defects in far-infrared reflectivity of $Ba(Mg_{1/3}Ta_{2/3})O_3$. *J Eur Ceram Soc* 2007;**27**:2797–802.
81. Shimada T, Ichikawa K, Minemura T, Kolodiazhnyi T, Breeze J, Alford NMcN, et al. Temperature and frequency dependence of dielectric loss of $BaMg_{1/3}Ta_{2/3}O_3$ microwave ceramics. *J Eur Ceram Soc* 2010;**30**:331–4.
82. Kolodiazhnyi T. Japanese Patent Application 2013-010006.
83. Kawashima S, Nishida M, Ueda T, Ouchi H. $BaZn_{1/3}Ta_{2/3}O_3$ ceramics with low dielectric loss at microwave frequencies. *J Am Ceram Soc* 1983;**66**:421–3.
84. Reaney IM, Wise PL, Qazi I, Miller CA, Price TJ, Cannell DS, et al. Ordering and quality factor in 0.95 $BaZn_{1/3}Ta_{2/3}O_3$-0.05$SrGa_{1/2}Ta_{1/2}O_3$ production resonators. *J Eur Ceram Soc* 2003;**23**:3021–34.
85. Tamura H, Konoike T, Sakabe Y, Wakino K. Improved high-Q dielectric resonator with complex perovskite structure. *J Am Ceram Soc* 1984;**67**. C-59-61.
86. Kageyama K. Crystal structure and microwave dielectric properties of $BaZn_{1/3}Ta_{2/3}O_3$-(Sr,Ba)$(Ga_{1/2}Ta_{1/2})O_3$ ceramics. *J Am Ceram Soc* 1992;**75**:1767–71.
87. Kolodiazhnyi T, Petric A, Belous AG, V'yunov O, Yanchevsky O. Synthesis and dielectric properties of barium tantalates and niobates with complex perovskite structure. *J Mater Res* 2002;**17**:3182–9.
88. Galasso F, Pinto J. Growth of single crystals of $Ba(B'_{0.33}Ta_{0.67})O_3$ perovskite-type compounds. *Nature* 1965;**207**:70–2.
89. Cervellino A, Gvasaliya SN, Roessli B, Rotaru GM, Cowley RA, Lushnikov SG, et al. Cube-shaped diffuse scattering and the ground state of $BaMg_{1/3}Ta_{2/3}O_3$. *Phys Rev B* 2012;**86**:104107.
90. Lu C-H, Tsai C-C. Reaction kinetics, sintering characteristics, and ordering behavior of microwave dielectrics: Barium magnesium tantalate. *J Mater Res* 1996;**11**:1219–27.
91. Lufaso MW. Crystal structures, modeling, and dielectric property relationships of 2:1 ordered $Ba_3MM'_2O_9$ (M = Mg, Ni, Zn; M′ = Nb, Ta) perovskites. *Chem Mater* 2004;**16**:2148–56.